






BRIEF DEFINITIVE REPORT

# GSDMD is critical for autoinflammatory pathology in a mouse model of Familial Mediterranean Fever

Apurva Kanneganti<sup>1,2,3,4,5</sup>, R.K. Subbarao Malireddi<sup>6</sup>, Pedro H.V. Saavedra<sup>1,2</sup> , Lieselotte Vande Walle<sup>1,2</sup>, Hanne Van Gorp<sup>1,2</sup>, Hiroto Kambara<sup>4,5</sup>, Heather Tillman<sup>7</sup>, Peter Vogel<sup>7</sup> , Hongbo R. Luo<sup>4,5</sup>, Ramnik J. Xavier<sup>3,8</sup> , Hongbo Chi<sup>6</sup> , and Mohamed Lamkanfi<sup>1,2</sup> 

**Pyroptosis is an inflammasome-induced lytic cell death mode, the physiological role of which in chronic inflammatory diseases is unknown. Familial Mediterranean Fever (FMF) is the most common monogenic autoinflammatory disease worldwide, affecting an estimated 150,000 patients. The disease is caused by missense mutations in *Mefv* that activate the Pyrin inflammasome, but the pathophysiological mechanisms driving autoinflammation in FMF are incompletely understood. Here, we show that *Clostridium difficile* infection of FMF knock-in macrophages that express a chimeric FMF-associated *Mefv*<sup>V726A</sup> Pyrin elicited pyroptosis and gasdermin D (GSDMD)-mediated interleukin (IL)-1 $\beta$  secretion. Importantly, in vivo GSDMD deletion abolished spontaneous autoinflammatory disease. GSDMD-deficient FMF knock-in mice were fully protected from the runted growth, anemia, systemic inflammatory cytokine production, neutrophilia, and tissue damage that characterize this autoinflammatory disease model. Overall, this work identifies pyroptosis as a critical mechanism of IL-1 $\beta$ -dependent autoinflammation in FMF and highlights GSDMD inhibition as a potential antiinflammatory strategy in inflammasome-driven diseases.**

## Introduction

Inflammasomes are intracellular multiprotein complexes that serve as platforms for activation of caspase-1 (Lamkanfi and Dixit, 2014; Man and Kanneganti, 2016). Pyroptosis is rapidly emerging as a key mechanism by which caspase-1 and the related inflammatory caspases-4, -5, and -11 contribute to host defense against bacterial infections (Jorgensen and Miao, 2015; Vande Walle and Lamkanfi, 2016). These inflammatory caspases induce pyroptosis by cleaving gasdermin D (GSDMD) at the central linker peptide, thereby separating the pore-forming amino-terminal domain (GSDMD<sub>N</sub>) from the inhibitory carboxy-terminal (GSDMD<sub>C</sub>) domain (Kayagaki et al., 2015; Shi et al., 2015; Aglietti et al., 2016; Ding et al., 2016). This cleavage event causes GSDMD<sub>N</sub> to oligomerize and insert in the plasma membrane, giving rise to a rapid loss of plasma membrane integrity and cell lysis. Pyroptosis deprives intracellular pathogens from their replicative niches and traps infectious agents in the cellular debris of infected cells to facilitate bacterial clearance by recruited neutrophils (Jorgensen et al., 2016). Moreover, it is thought to promote the extracellular release of the nuclear alarmin HMGB1 and

the inflammatory cytokines IL-1 $\beta$  and IL-18 during infections (Lamkanfi et al., 2010; Kayagaki et al., 2015; Shi et al., 2015). Akin to GSDMD, IL-1 $\beta$  and IL-18 are inflammasome substrates that are produced as biologically inert precursor proteins that are stored in the cytosol until they undergo proteolytic conversion into the mature, secreted cytokines after inflammasome assembly. Contrary to GSDMD, however, pro-IL-1 $\beta$  and pro-IL-18 are specifically cleaved by caspase-1, but not other inflammatory caspases.

As key regulators of both innate and adaptive immunity, IL-1 $\beta$  and IL-18 not only are central to coordinating antimicrobial host defense, but these cytokines also play central roles in autoimmune and autoinflammatory diseases (Garlanda et al., 2013; Gurung and Kanneganti, 2016; Van Gorp et al., 2017). Familial Mediterranean fever (FMF) is the most prevalent monogenic autoinflammatory disease worldwide, and it has a particularly high prevalence of 1:500 to 1:1,000 among individuals of Middle Eastern and Mediterranean descent (Ozen and Bilginer, 2014). The large majority of FMF patients carry mutations in the carboxy-terminal B30.2 (PRY/SPRY) domain of the human inflammasome sensor Pyrin,

<sup>1</sup>Center for Inflammation Research, Vlaams Instituut voor Biotechnologie, Ghent, Belgium; <sup>2</sup>Department of Internal Medicine, Ghent University, Ghent, Belgium; <sup>3</sup>Gastrointestinal Unit, Center for Computational and Integrative Biology, Massachusetts General Hospital, Harvard Medical School, Boston, MA; <sup>4</sup>Department of Pathology, Harvard Medical School, Boston, MA; <sup>5</sup>Department of Lab Medicine, Boston Children's Hospital, Dana-Farber/Harvard Cancer Center, Boston, MA; <sup>6</sup>Department of Immunology, St. Jude Children's Research Hospital, Memphis, TN; <sup>7</sup>Department of Pathology, St. Jude Children's Research Hospital, Memphis, TN; <sup>8</sup>Broad Institute of Harvard and MIT, Cambridge, MA.

Correspondence to Mohamed Lamkanfi: [mlamkanf@its.jnj.com](mailto:mlamkanf@its.jnj.com); M. Lamkanfi's present address is Janssen Immunosciences, World Without Disease Accelerator, Janssen Pharmaceutica, Pharmaceutical Companies of Johnson & Johnson, Beerse, Belgium.

© 2018 Kanneganti et al. This article is distributed under the terms of an Attribution–Noncommercial–Share Alike–No Mirror Sites license for the first six months after the publication date (see <http://www.rupress.org/terms/>). After six months it is available under a Creative Commons License (Attribution–Noncommercial–Share Alike 4.0 International license, as described at <https://creativecommons.org/licenses/by-nc-sa/4.0/>).

encoded by *Mefv* (Ozen and Bilginer, 2014), and the field has recently witnessed tremendous progress in understanding the mechanisms regulating activation of the Pyrin inflammasome (Xu et al., 2014; Gao et al., 2016; Masters et al., 2016; Park et al., 2016; Van Gorp et al., 2016). FMF mutations in the carboxy-terminal B30.2 domain were recently demonstrated to render Pyrin inflammasome activation independent of microtubules (Van Gorp et al., 2016), but the physiological mechanisms driving FMF pathogenesis are still largely unknown. An important hurdle for modeling FMF in preclinical animal models is that the rodent orthologue of human Pyrin lacks the carboxy-terminal B30.2 (PRY/SPRY) domain that is frequently mutated in FMF patients. However, previous studies showed that knock-in mice engineered to express a chimeric Pyrin protein from the endogenous *Mefv* locus that is composed of full-length mouse Pyrin and an FMF-associated mutant human B30.2 domain spontaneously develop IL-1 receptor-dependent autoinflammation that is rescued by deletion of the central inflammasome adaptor protein ASC (Chae et al., 2011). In agreement with clinical evidence showing a detrimental role for IL-1 $\beta$  production in FMF patients (Ozdogan and Ugurlu, 2017), autoinflammatory pathology in these knock-in mice expressing the common *Mefv*<sup>V726A</sup> FMF mutation was selectively driven by IL-1 $\beta$ , but not IL-1 $\alpha$  (Sharma et al., 2017). Considering the key role of IL-1 $\beta$  in FMF and other inflammatory diseases, a key outstanding question is what mechanisms are responsible for IL-1 $\beta$  secretion under conditions that promote chronic inflammatory disease. Numerous mechanisms for secretion of IL-1 $\beta$  have been proposed in this respect, including lysosomal exocytosis (Andrei et al., 1999), exosome exocytosis (Qu et al., 2007), microvesicle shedding (MacKenzie et al., 2001), and alternative inflammasome activation (Gaidt et al., 2016), but studies addressing the physiological roles of these IL-1 $\beta$  secretory pathways in autoinflammatory and autoimmune disease in vivo have not been reported.

Here, we explore the hypothesis that IL-1 $\beta$ -dependent autoinflammation in the *Mefv*<sup>V726A/V726A</sup> FMF mouse model is driven by pyroptotic cytokine release. We showed that the pyroptosis effector GSDMD is cleaved concomitantly with IL-1 $\beta$  in ex vivo-cultured *Mefv*<sup>V726A/V726A</sup> macrophages that had been infected with *Clostridium difficile* and that GSDMD deletion dampens extracellular release of IL-1 $\beta$ . Importantly, we demonstrate that in vivo GSDMD deletion fully rescued autoinflammation-associated growth retardation, anemia, cytokine production, neutrophilia, and tissue damage in *Mefv*<sup>V726A/V726A</sup> FMF mice. Overall, this work establishes pyroptosis as a critical in vivo mechanism of autoinflammation and thus suggests that pyroptosis inhibition may prevent inflammasome-dependent autoinflammatory and autoimmune pathology.

## Results and discussion

### Pyroptosis contributes to IL-1 $\beta$ secretion ex vivo from *C. difficile*-infected *Mefv*<sup>V726A/V726A</sup> macrophages

Bone marrow-derived macrophages (BMDMs) of *Mefv*<sup>V726A/V726A</sup> mice were infected with *C. difficile* to analyze inflammasome-induced maturation of caspase-1 and the pyroptosis executioner GSDMD because this Gram-positive, toxin-producing bacterial

pathogen was recently shown to activate the Pyrin inflammasome in human peripheral blood mononuclear cells (PBMCs) and mouse macrophages (Van Gorp et al., 2016). Unlike in noninfected cells, significant cleavage of caspase-1 and GSDMD was observed in *C. difficile*-infected BMDMs (Fig. 1 A). Consistent with potent Pyrin inflammasome activation under these experimental conditions, we detected significant levels of secreted IL-1 $\beta$  in the culture supernatants (Fig. 1 B). *C. difficile* infection also triggered robust induction of cell death, with nearly all *Mefv*<sup>V726A/V726A</sup> macrophages being labeled by the cell-impermeant fluorescent dye Sytox green 25 h after infection (Fig. 1 C). The cell death response was pyroptotic in nature because genetic deletion of GSDMD markedly diminished the fraction of Sytox green-positive *Mefv*<sup>V726A/V726A</sup> macrophages after *C. difficile* infection (Fig. 1 C). Moreover, pyroptosis contributed to IL-1 $\beta$  secretion because culture supernatants of GSDMD-deficient *Mefv*<sup>V726A/V726A</sup> macrophages contained significantly less IL-1 $\beta$  than GSDMD-sufficient cells when probed at 8 h and 20 h after infection, respectively (Fig. 1, D and E). Western blotting analysis of culture supernatants and whole cell lysates confirmed that *Mefv*<sup>V726A/V726A</sup> *Gsdmd*<sup>-/-</sup> macrophages matured IL-1 $\beta$ , which mostly was retained intracellularly, whereas the bulk of the mature cytokine was retrieved in the culture medium of GSDMD-sufficient *Mefv*<sup>V726A/V726A</sup> macrophages (Fig. 1 F). Although GSDMD deletion did not abolish cytokine secretion, these results identify pyroptosis as an important mechanism contributing to IL-1 $\beta$  secretion from ex vivo-infected *Mefv*<sup>V726A/V726A</sup> macrophages. Because GSDMD-deficient macrophages were shown to undergo apoptosis after inflammasome activation (He et al., 2015), it is likely that residual TcdA-induced IL-1 $\beta$  release from GSDMD-deficient macrophages could be associated with induction of secondary necrosis after apoptotic cell death ex vivo.

### Pyroptosis is essential for systemic IL-1 $\beta$ release and inflammatory cytokine production in vivo

Recurrent fever and systemic autoinflammation appear unprovoked and are not associated with infections in FMF patients. To address the in vivo role of pyroptosis in secretion of IL-1 $\beta$  in a more physiologically relevant context of autoinflammation, we measured the levels of IL-1 $\beta$  in serum of *Mefv*<sup>V726A/V726A</sup> mice that were either sufficient or deficient in GSDMD expression. Consistent with previous studies (Chae et al., 2011; Sharma et al., 2017), we measured significant levels of IL-1 $\beta$  in serum of 4- to 7-wk-old *Mefv*<sup>V726A/V726A</sup> mice, but not in heterozygous littermate control mice (Fig. 2 A). Notably, deletion of GSDMD fully abolished in vivo IL-1 $\beta$  production in serum of *Mefv*<sup>V726A/V726A</sup> mice aged 4–7 wk (Fig. 2 A), which contrasted markedly to the continued release of IL-1 $\beta$  in culture media of BMDMs that had been infected with *C. difficile* ex vivo (Fig. 1). *Mefv*<sup>V726A/V726A</sup> mice aged 10 wk and older continued to present with high IL-1 $\beta$  concentrations in their blood, whereas pyroptosis-deficient littermate mice had only background IL-1 $\beta$  levels (Fig. 2 A), identifying pyroptosis as the central mechanism of chronic IL-1 $\beta$  release in the circulation of *Mefv*<sup>V726A/V726A</sup> mice. Because *Mefv*<sup>V726A/V726A</sup> mice were shown to produce a suite of inflammatory cytokines and chemokines in an IL-1 $\beta$ -dependent manner (Sharma et al., 2017), we further examined how GSDMD deficiency impacts on

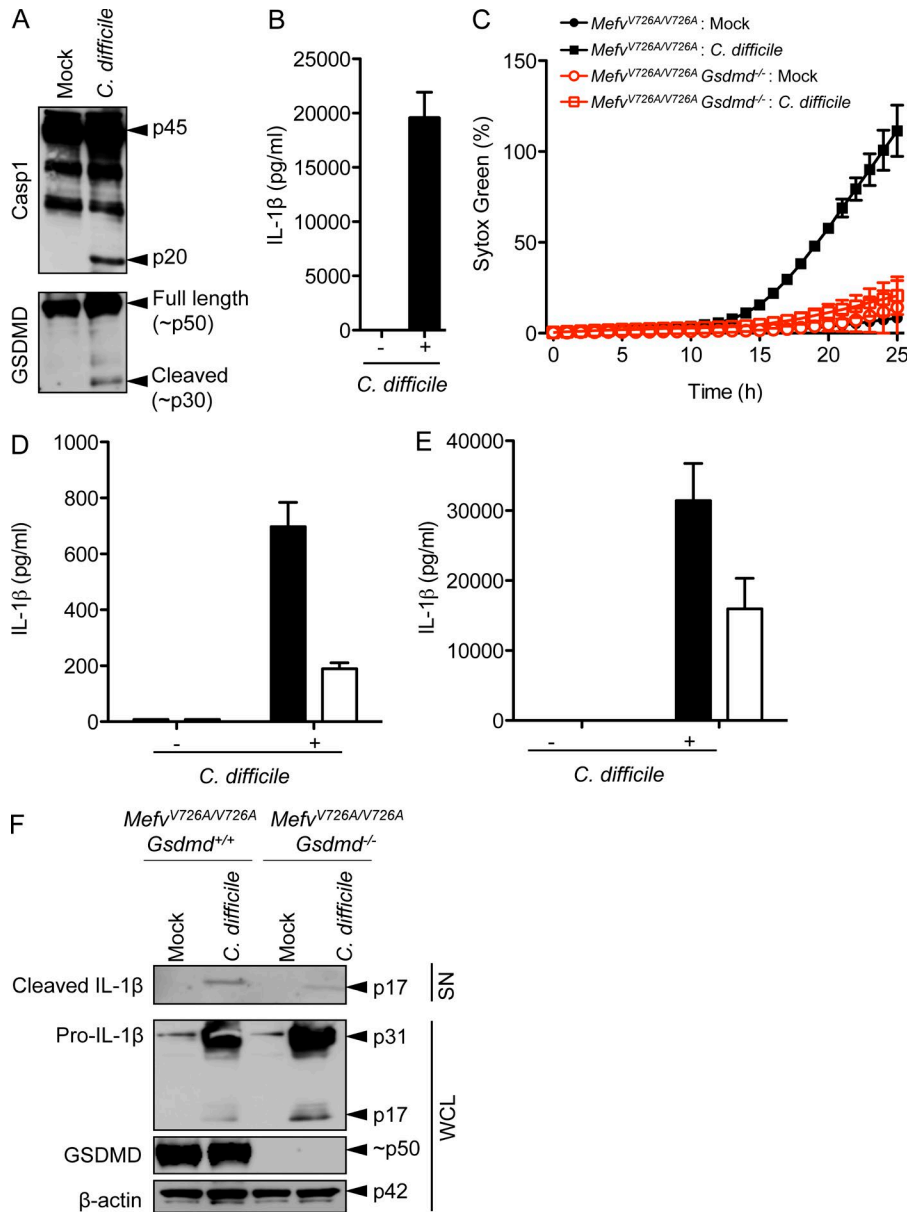


**Figure 1. Pyroptosis contributes to IL-1 $\beta$  secretion from ex vivo *C. difficile*-infected *Mefv<sup>V726A/V726A</sup>* macrophages. (A and B)** BMDMs from *Mefv<sup>V726A/V726A</sup>* mice were infected with *C. difficile* (10 MOI) for 20 h. Cell lysates were immunoblotted for caspase-1 and GSDMD (A), and culture supernatants were analyzed for IL-1 $\beta$  (B). **(C–E)** BMDMs from *Mefv<sup>V726A/V726A</sup>* and *Mefv<sup>V726A/V726A</sup>* *Gsdmd<sup>-/-</sup>* littermate mice were infected with *C. difficile* (10 MOI), and induction of pyroptosis was quantified over time by monitoring Sytox green incorporation (C). Culture supernatants were analyzed for IL-1 $\beta$  levels at 8 h (D) and 20 h (E) after infection. **(F)** BMDMs were infected with *C. difficile* during 8 h before culture supernatants (SN) and whole cell lysates (WCL) were immunoblotted for IL-1 $\beta$ , GSDMD, and  $\beta$ -actin. Bands are denoted with black arrows and the corresponding size. All data are representative of three independent experiments, and cytokine data are presented as mean  $\pm$  SD from a representative experiment out of three performed with  $n = 3$  in each repeat. p in Western blots denotes protein molecular weight.

serum levels of a panel of inflammatory cytokines and chemokines. GSDMD deletion abrogated IL-1 $\beta$ -dependent production of IL-6, TNF, IL-18, IL-17A, RANTES, MCP-1, IFN- $\gamma$ , IP-10, G-CSF, and other inflammatory mediators in *Mefv<sup>V726A/V726A</sup>* mice (Fig. S1), further supporting the critical role of pyroptosis in systemic IL-1 $\beta$  release and autoinflammation-associated cytokine production. Consistent with Pyrin inflammasome activation in vivo, we found that caspase-1 and GSDMD were constitutively activated in peritoneal macrophages and circulating monocytes of *Mefv<sup>V726A/V726A</sup>* mice, but not in cells of *Mefv<sup>V726A/+</sup>* littermate mice (Fig. 2, B and C). Ex vivo incubation of isolated peritoneal macrophages and blood monocytes in culture media further enhanced cleavage of caspase-1 and GSDMD. We similarly observed constitutive activation of the Pyrin inflammasome in granulocytes of *Mefv<sup>V726A/V726A</sup>* mice, unlike in the neutrophilic fraction of *Mefv<sup>V726A/+</sup>* littermate mice (Fig. S2). Together, these results demonstrate that FMF-associated mutations in *Mefv*

promote constitutive Pyrin inflammasome activation, GSDMD maturation, and pyroptosis-dependent systemic inflammation in *Mefv<sup>V726A/V726A</sup>* mice.

### Pyroptosis causes neutrophilia, runting, and wasting disease in *Mefv<sup>V726A/V726A</sup>* mice

To further assess the role of GSDMD in IL-1 $\beta$ -mediated autoinflammation, we examined signs of systemic neutrophilia, which is typically involved in the clinical manifestation of FMF (Ozen and Bilginer, 2014). Consistent with reported findings (Chae et al., 2011; Sharma et al., 2017), flow cytometry analysis indicated that *Mefv<sup>V726A/V726A</sup>* mice had a markedly increased proportion of Gr-1<sup>+</sup>CD11b<sup>+</sup> polymorphonuclear leukocytes (PMNs) in their blood (Fig. 3 A). Absolute PMN counts were also increased in autoinflammatory *Mefv<sup>V726A/V726A</sup>* mice (Fig. 3 B), consistent with the systemic neutrophilia seen in FMF patients. Mice lacking GSDMD on either a wild-type or

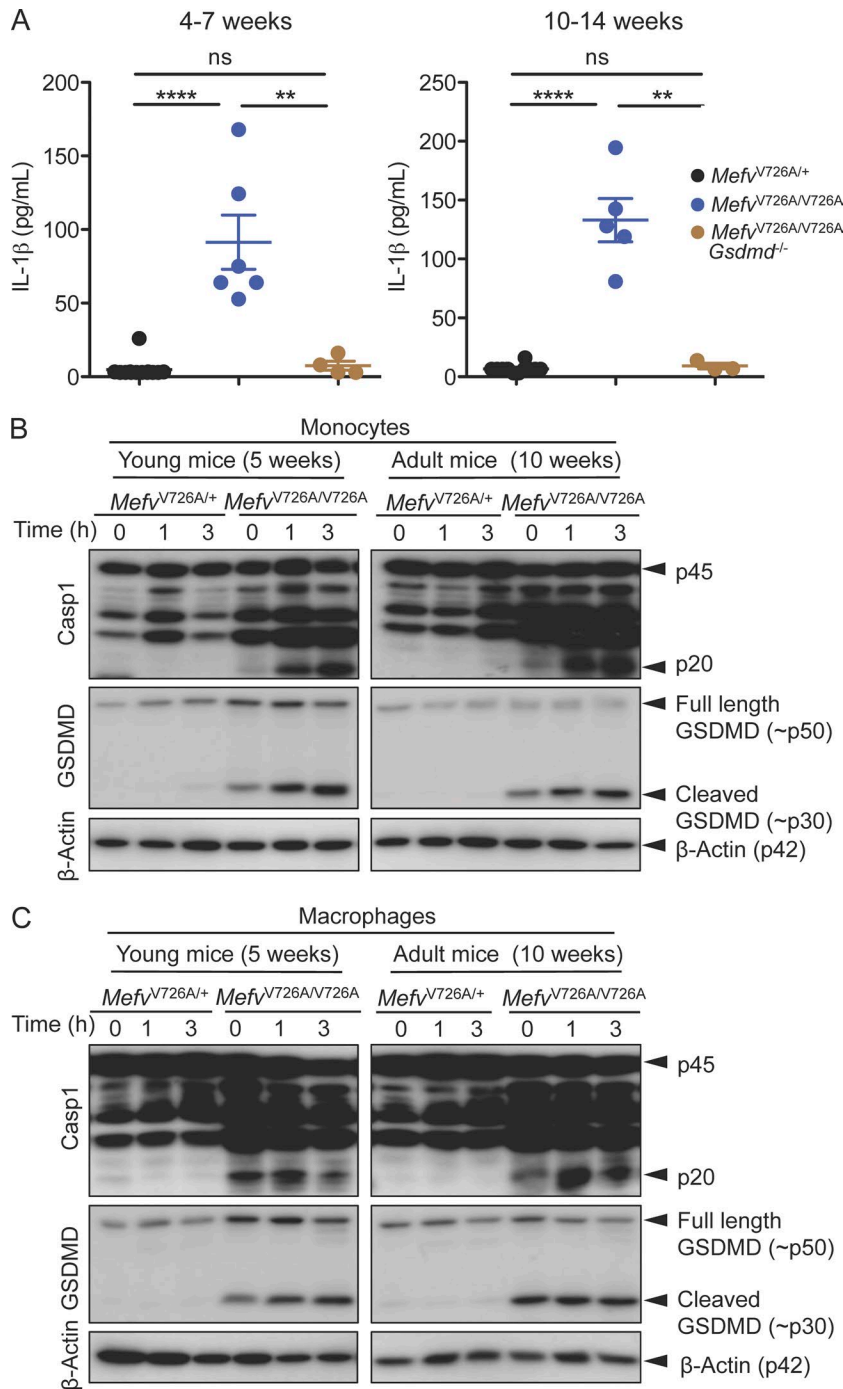


**Figure 2. Pyrin-induced pyroptosis is essential for systemic IL-1 $\beta$  secretion in *Mefv*<sup>V726A/V726A</sup> mice. (A)** Levels of IL-1 $\beta$  in serum samples taken from littermate mice of the indicated genotypes that were aged 4–7 wk and 10–14 wk at the time of analysis. Data are presented as mean  $\pm$  SEM with  $n = 4$ –13 for each genotype. Data points are color coded according to the mouse genotypes shown in the corresponding figure legend.  $P < 0.05$  is considered statistically significant. \*\*,  $P < 0.01$  and \*\*\*\*,  $P < 0.0001$  using unpaired Student's  $t$  test and two-tailed  $p$ -values. ns, not significant. **(B and C)** Blood monocytes and peritoneal macrophages from littermate mice of the indicated genotypes and age were immunoblotted for caspase-1, GSDMD, and  $\beta$ -actin upon collection or after incubation in culture media for the indicated duration. Data are representative for three independent experiments. p in Western blots denotes protein molecular weight. Data are representative of three independent experiments with  $n = 3$  in each repeat (B and C).

autoinflammatory *Mefv*<sup>V726A/V726A</sup> genetic background were indistinguishable from heterozygous *Mefv*<sup>V726A/+</sup> control mice, presenting with baseline neutrophil counts (Fig. 3, A and B). *Mefv*<sup>V726A/V726A</sup> mice and littermate mice that lacked GSDMD expression were scored regularly for clinical markers of disease progression, including body weight, skin scaling, and runting at weaning (when aged 4 wk) until they became 9 wk old. As expected (Chae et al., 2011; Sharma et al., 2017), from the onset of our measurements and continued throughout the observed period, *Mefv*<sup>V726A/V726A</sup> mice did display a markedly lower body weight as compared with that of heterozygous *Mefv*<sup>V726A/+</sup>

control mice (Fig. 3 C). In sharp contrast, *Mefv*<sup>V726A/V726A</sup> mice that lacked GSDMD expression presented with normal body weight (Fig. 3 C) and appeared fully protected from runting, skin lesions, tail deformities, and muscle wasting that was readily seen in autoinflammatory *Mefv*<sup>V726A/V726A</sup> mice (Fig. 3 D and not depicted). Moreover, defective pyroptosis induction fully protected *Mefv*<sup>V726A/V726A</sup> mice from anemia, as evident from measurement of blood hemoglobin and hematocrit levels (Fig. 3 E). Together, these results identify pyroptosis as a key mechanism driving the clinical pathogenesis of IL-1 $\beta$ -mediated autoinflammatory disease.

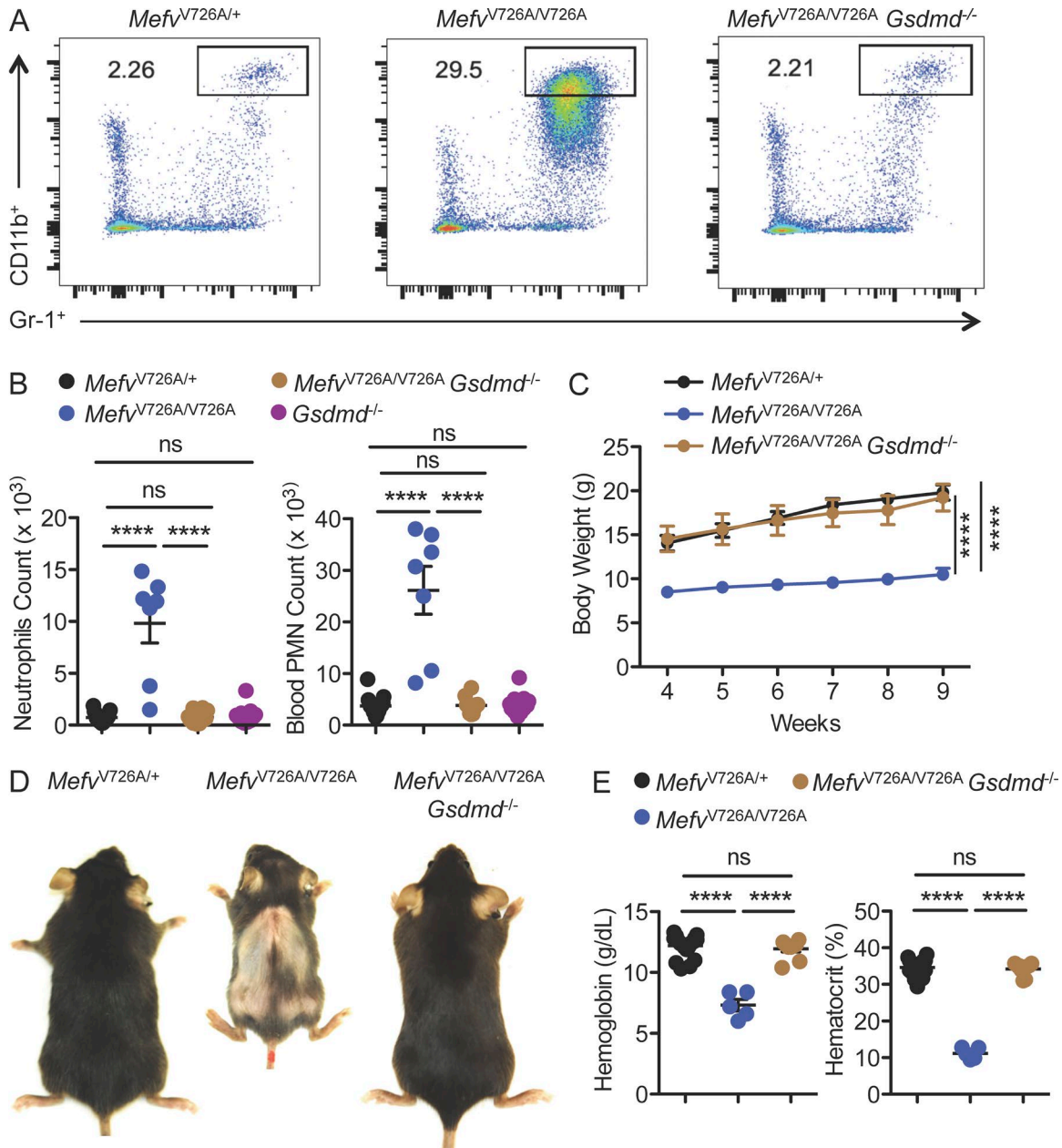


**Figure 3. GSDMD promotes neutrophilia, runting, and wasting disease in *Mefv*<sup>V726A/V726A</sup> mice.** (A) Representative dot plot depicting the proportion of neutrophils (CD11b<sup>+</sup>Gr1<sup>+</sup>), distinguished by high CD11b<sup>+</sup> values, in blood of littermate mice of the indicated genotypes. The percentage of cells identified as neutrophils is depicted on each plot. (B) Levels of neutrophils and PMNs in blood of littermate mice and nonlittermate GSDMD knockout mice. Data are presented as mean ± SEM with *n* = 7–17 for each genotype. (C) Body weight of female littermate mice of the indicated genotypes was analyzed weekly when mice were 4 wk old until aged 9 wk. Data are presented as mean ± SEM with *n* = 5–14 for each genotype. (D) Representative photos of littermate mice of the indicated genotypes are shown. (E) Levels of hemoglobin and hematocrit are shown as a measure of anemia in littermate mice of the indicated genotypes. Data are presented as mean ± SEM with *n* = 5–20 for each genotype. Data points are color coded according to the mouse genotypes shown in the corresponding figure legend. *P* < 0.05 is considered statistically significant. \*\*\*\*, *P* < 0.0001 using unpaired Student's *t* test and two-tailed *p*-values (B, C, and E). Data are representative of two independent experiments (A–E). ns, not significant.

***Mefv*<sup>V726A/V726A</sup>-associated histopathology is dependent on GSDMD**

Neutrophilia in FMF usually is accompanied by leukocyte infiltration and splenomegaly. These disease traits were all observed in *Mefv*<sup>V726A/V726A</sup> mice, but genetic deletion of GSDMD fully prevented splenomegaly (Fig. 4 A), as also confirmed by comparison of spleen weight of the respective genotypes (Fig. 4 B). Moreover, the loss of GSDMD protected *Mefv*<sup>V726A/V726A</sup> mice against

all observed histological perturbations, including evidence of multifocal moderate hepatitis in the liver, multifocal moderate glomerulonephritis in the kidney, diffuse moderate to marked colitis in the colon, diffuse moderate intravascular granulocytosis in the lung, and diffuse marked granulocytopenia and markedly reduced erythropoiesis in bone marrow and diffuse marked periarticular suppurative inflammation in the knee (Fig. 4 C). *Mefv*<sup>V726A/V726A</sup> mice also displayed signs of organ damage such

as bile duct hyperplasia in the liver, glomerulopathy, necrosis, and proteinosis in the kidney and mucosal hyperplasia in the colon. Histological scoring by an experienced pathologist who was blinded to the experimental groups confirmed that these clinical features of organ damage were fully rescued by genetic deletion of GSDMD (Fig. S3).

Histological analysis of H&E-stained spleen sections further revealed that GSDMD deletion blunted the extramedullary hematopoiesis and normalized the aberrant morphology of the periarteriolar lymphoid sheaths and follicle regions in the white pulp areas of *Mefv<sup>V726A/V726A</sup>* spleens (unpublished data). To study these changes in additional detail, we performed immunohistochemical analysis of spleen sections to characterize splenocyte cell types and distribution. The white pulp areas of the spleen normally contain T cells in the periarteriolar lymphoid sheaths and B cells in the follicles. However, these areas were indistinct in spleens of *Mefv<sup>V726A/V726A</sup>* mice and showed evidence of plasma cell hyperplasia, including an abundant presence of IRF4<sup>+</sup> plasma cells containing large globules of immunoglobulins that are known as Mott cells (Fig. 5, A and B). This was accompanied by marked decreases in numbers of B220<sup>+</sup> B cells, CD4<sup>+</sup> T cells, and CD8<sup>+</sup> T cells. Macrophage counts in the spleens of *Mefv<sup>V726A/V726A</sup>* mice did not differ notably from those seen in heterozygous control mice, but their macrophages displayed an activated morphology that was characterized by a more amoeboid and less dendritic cytoplasm and an enlarged nucleus (unpublished data). The increased erythropoiesis in the spleens of *Mefv<sup>V726A/V726A</sup>* mice is most likely a result of displacement by increased granulocytosis in the bone marrow. Notably, these alterations were all absent in spleens of *Mefv<sup>V726A/V726A</sup> Gsdmd<sup>-/-</sup>* mice (Fig. 5, A and B). Altogether, these results support the concept that GSDMD drives the clinical manifestation of FMF-associated pathology by promoting pyroptotic release of IL-1 $\beta$ .

IL-1 $\beta$  is a pleiotropic cytokine that plays a central role in coordinating inflammatory, wound-healing, and antimicrobial host defense responses during infections. However, unabated and chronic IL-1 $\beta$  production may also be pathogenic to patients, as illustrated by the remarkable efficacy of approved IL-1 $\beta$ -neutralizing biologics in patients suffering from a suite of arthritic and autoinflammatory diseases (Hoffman and Broderick, 2016). Moreover, results from a recent multicentered, double-blind, placebo-controlled clinical study further highlighted the detrimental role of chronic IL-1 $\beta$  production in postinfarction heart failure in patients with inflammatory atherosclerosis (Ridker et al., 2017a), and other findings suggest that IL-1 $\beta$  neutralization might significantly reduce the risk for lung cancer and lung cancer-associated mortality (Ridker et al., 2017b). Several mechanisms that control IL-1 $\beta$  secretion have been put forward, including lysosomal exocytosis (Andrei et al., 1999), exosome exocytosis (Qu et al., 2007), microvesicle shedding (MacKenzie et al., 2001), and alternative inflammasome activation (Gaidt et al., 2016), but studies addressing their roles in autoinflammation and autoimmunity have not been reported.

Here, we demonstrated that pyroptosis partially accounts for IL-1 $\beta$  secretion from *Mefv<sup>V726A/V726A</sup>* macrophages that have been infected *ex vivo* with the Gram-positive bacterial pathogen *C. difficile*, suggesting that additional mechanisms

contribute to IL-1 $\beta$  secretion under these experimental conditions. Remarkably, however, genetic deletion of the central pyroptosis effector protein GSDMD fully rescued autoinflammatory *Mefv<sup>V726A/V726A</sup>* mice from spontaneous IL-1 $\beta$ -driven autoinflammatory pathology. GSDMD deficiency not only ablated circulating levels of IL-1 $\beta$ , but fully protected against all clinical hallmark symptoms of autoinflammatory pathology in *Mefv<sup>V726A/V726A</sup>* mice, including runting, anemia, inflammatory cytokine and chemokine secretion, neutrophilia, splenomegaly, and systemic tissue damage. Thus, we have shown a crucial role for pyroptosis in driving autoinflammatory pathology in FMF. This work thus clearly delineates the dominant contribution of GSDMD-mediated pyroptosis to IL-1 $\beta$ -dependent pathology in this mouse model of FMF-associated autoinflammation and suggests that pyroptosis may similarly exert a crucial role in the etiology of other chronic IL-1 $\beta$ -mediated autoinflammatory and autoimmune diseases. Analogous studies to the ones presented here may shed light on the relative contribution of GSDMD and pyroptosis to additional IL-1 $\beta$ -dependent autoinflammatory and autoimmune pathologies, including cryopyrin-associated periodic syndromes (Brydges et al., 2009) and spontaneous HA20-associated inflammatory arthritis in mice with a myeloid-restricted deletion of A20/TNFAIP3 (Vande Walle et al., 2014). Additionally, exploration of the role of pyroptosis in autoimmune and autoinflammatory diseases associated with high circulating levels of IL-18 and DAMPs, such as S100 proteins and HMGB1, is warranted. Such studies might further highlight the potential of pyroptosis inhibition as an anti-inflammatory strategy in diverse chronic diseases.

## Materials and methods

### Mice

We thank D.L. Kastner (National Institutes of Health, Bethesda, MD) for providing *Mefv<sup>V726A/+</sup>* mice and V.M. Dixit and N. Kayagaki (Genentech, South San Francisco, CA) for providing *Gsdmd<sup>-/-</sup>* mice (Chae et al., 2011; Kayagaki et al., 2015). *Mefv<sup>V726A/+</sup>* mice were bred to *Gsdmd<sup>-/-</sup>* mice to generate *Mefv<sup>V726A/V726A</sup> GSDMD<sup>-/-</sup>* mice. Mice were housed in individually ventilated cages and were maintained in specific pathogen-free facilities of Ghent University and St. Jude Children's Research Hospital. Animal studies were approved by the ethics committees on laboratory animal welfare of Ghent University and St. Jude Children's Research Hospital Committees on the Use and Care of Animals.

### Tissue processing and analysis

Mice were monitored weekly for weight gain starting from 4 wk of age and euthanized when aged 8–12 wk for systemic analyses. Blood was collected through cardiac puncture and retroorbital bleeding, and 50  $\mu$ l was added to anticoagulant EDTA for cellular analysis. The spleen was homogenized and passed through a 40- $\mu$ m filter to obtain a single-cell suspension. Both blood and spleen were subjected to RBC lysis and washed in complete media. Left lobes of lung were homogenized, filtered, and subjected to a 33% Percoll (GE) gradient centrifugation to remove debris and obtain single cell suspension.

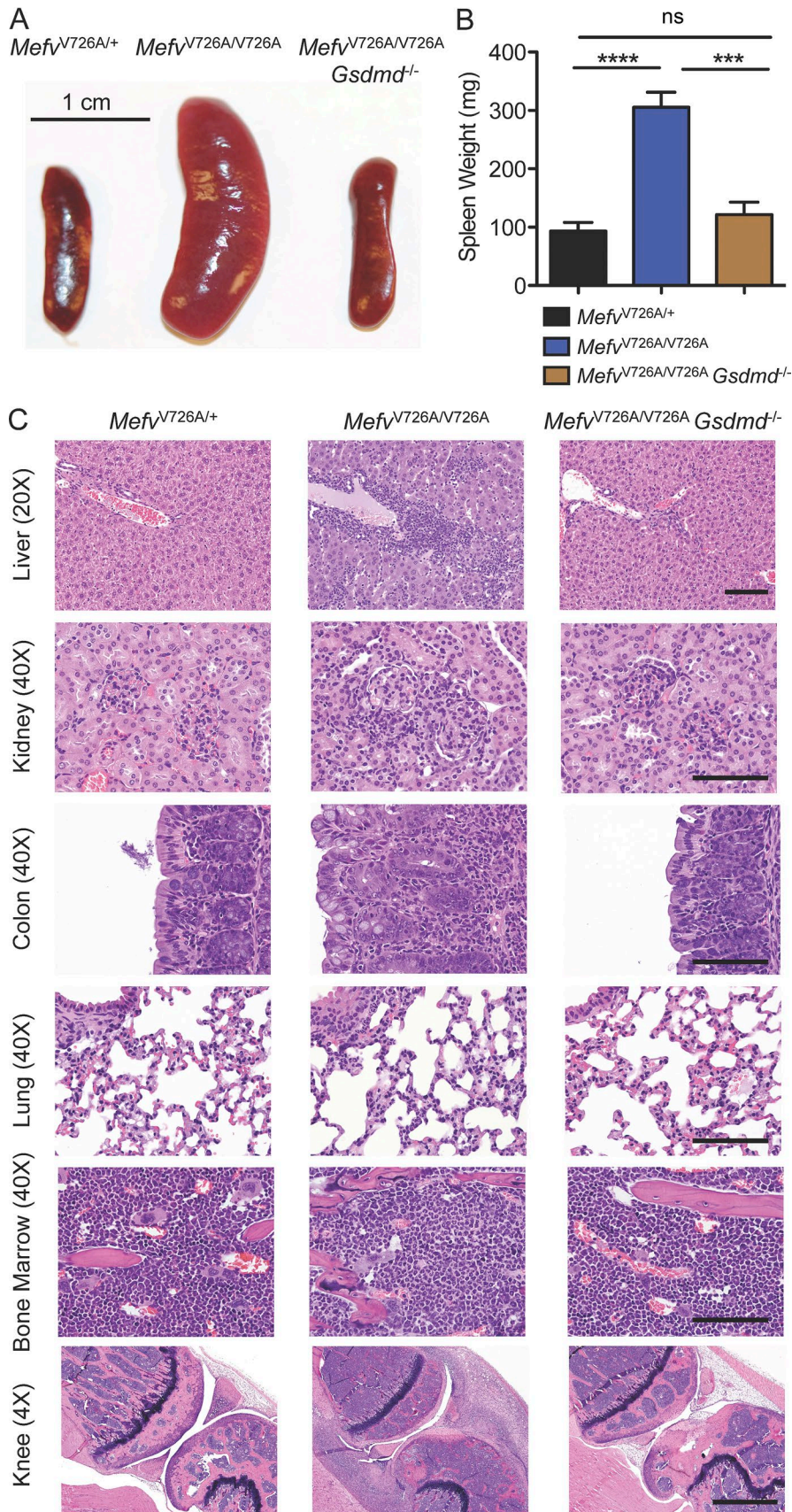


**Figure 4. Autoinflammation-associated histopathology in *Mefv*<sup>V726A/V726A</sup> mice is dependent on GSDMD.** (A and B) Representative photos; bar represents 1 cm (A) and weight (B) of spleens of littermate mice of the indicated genotypes. Spleen weight is presented as mean ± SEM with *n* = 3–4 for each genotype. Bar graph is color coded according to the mouse genotypes shown in the corresponding figure legend. *P* < 0.05 is considered statistically significant. \*\*\*, *P* < 0.001 and \*\*\*\*, *P* < 0.0001 using unpaired Student's *t* test and two-tailed *p*-values. ns, not significant. (C) Representative sections of H&E-stained liver, kidney, colon, lung, bone marrow, and knee tissue are shown. Bars: (liver, kidney, colon, lung, and bone marrow) 50 μm; (knee) 500 μm. Original magnification is indicated. Histology scores are provided in Fig. S3. Data are representative of two independent experiments (A–C).

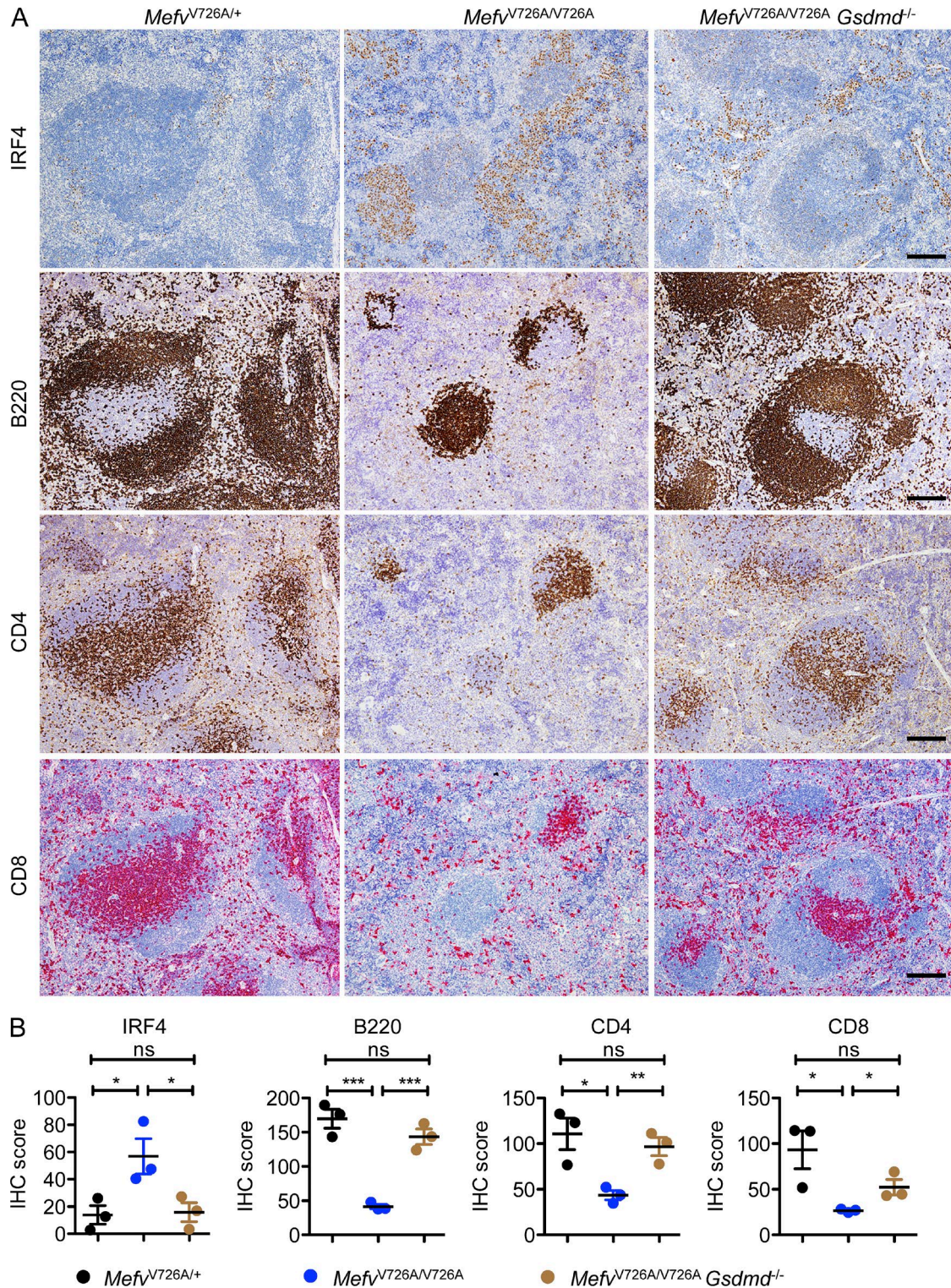


Figure 5. **Pyroptosis drives altered splenocyte cell types and distribution in *Mefv*<sup>V726A/V726A</sup> mice.** (A) The organization and cell types of the spleen of littermate mice of the indicated genotypes was compared by immunohistochemistry with antibodies against plasma cells (IRF4), B cells (B220), and T cells (CD4 and CD8). Representative micrographs are shown. Bars, 50  $\mu$ m in all panels. (B) Scoring of IHC slides that were digitized using an Aperio ScanScope XT (Leica Biosystems) for quantifying the areas of IRF4, B220, CD4, and CD8 labeling in serial sections of the spleens and to measure the areas of the spleens and splenic follicles. Bars are color coded according to the mouse genotypes shown in the corresponding figure legend. \*,  $P < 0.05$  (considered statistically significant); \*\*,  $P < 0.01$ ; and \*\*\*,  $P < 0.001$  using unpaired Student's *t* test and two-tailed *p*-values. ns, not significant. Data are representative of two independent experiments with  $n = 3$  for each group (A and B).



### Flow cytometry

The following antibodies were used for cell surface staining: CD11b (M1/70), CD19 (6D5), CD3 (17A2), and Gr-1 (RB6-8C5; all from eBiosciences). Cells were stained, run on LSRII flow cytometer (BD Biosciences), and analyzed with FlowJo software version 10.2 (FlowJo LLC). After removal of doublets, B cells were gated as CD19<sup>+</sup> and T cells as CD3<sup>+</sup>; CD11b<sup>+</sup> and PMN (CD11b<sup>+</sup>Gr1<sup>+</sup>) were gated on cells negative for both CD3 and CD19.

### Histology and immunohistochemistry

All tissues were fixed in formalin, embedded in paraffin, sectioned at 5  $\mu$ m, mounted on positively charged glass slides (Superfrost Plus; Thermo Fisher Scientific), and dried at 60°C for 20 min before dewaxing and staining with H&E using standard methods. H&E-stained sections were examined by a pathologist blinded to the experimental group assignments. Scores were assigned based on inflammation, ulceration, hyperplasia, and the extent or severity of damage. Severity scores for colon inflammation were assigned as follows: 0 = normal (within normal limits); 2 = minimal (mixed inflammation, small, focal, or widely separated, limited to lamina propria); 15 = mild (multifocal mixed inflammation, often extending into submucosa); 40 = moderate (large multifocal lesions within mixed inflammation involving mucosa and submucosa); 80 = marked (extensive mixed inflammation with edema and erosions); 100 = severe (diffuse inflammation with transmural lesions and multiple ulcers). Scores for ulceration were assigned as follows: 0 = normal (none); 2 = minimal (only one small focus of ulceration involving <5 crypts); 15 = mild (a few small ulcers up to 5 crypts); 40 = moderate (multifocal ulcers up to 10 crypts); 80 = marked (multifocal to coalescing ulcers involving >10 crypts each); 100 = severe (extensive to diffuse with multiple ulcers covering >20 crypts each). Scores of hyperplasia were assigned as follows: 0 = normal; 2 = minimal (some areas with crypts elongated and increased mitoses); 15 = mild (multifocal areas with crypts elongated up to twice the normal thickness, normal goblet cells present); 40 = moderate (extensive areas with crypts up to twice the normal thickness, reduced goblet cells); 80 = marked (mucosa over twice the normal thickness, hyperchromatic epithelium, reduced or rare goblet cells, possibly foci of arborization); 100 = severe (mucosa twice the normal thickness, marked hyperchromasia, crowding or stacking, absence of goblet cells, high mitotic index and arborization). Scores of extents were assigned as follows: 0 = normal (rare or inconspicuous lesions); 2 = minimal (<5% involvement); 15 = mild (multifocal but conspicuous lesions, 5–10% involvement); 40 = moderate (multifocal, prominent lesions, 10–50% involvement); 80 = marked (coalescing to extensive lesions or areas of inflammation with some loss of structure, 50–90% involvement); 100 = severe (diffuse lesion with effacement of normal structure, >90% involvement).

For immunohistochemical staining of the spleen, the primary antibodies used in this study included the following: for plasma cells, anti-IRF4 (1:300 dilution; sc-6059; Santa Cruz Biotechnology); for B cells, anti-B220 (1:1,000 dilution; 553084; BD PharMingen); and for T cells, anti-CD4 (4SM95; 1:40 dilution; 14-9766; Thermo Fisher Scientific) and anti-CD8 (1:40 dilution; 14-0808-82; Thermo Fisher Scientific). For detection of CD4 and

B220, sections underwent antigen retrieval at 100°C for 20 min in Epitope Retrieval solution 2 on a Bond Max immunostainer (Leica Biosystems). Then biotinylated secondary rabbit anti-rat antibody diluted 1:400 (BA-4001; Vector Laboratories) was applied for 10 min followed by Bond polymer refine detection kit with 3,3'-diaminobenzidine (DAB) as chromogenic substrate and a hematoxylin counterstain (DS9800; Leica Biosystems). For detection of IRF4, CD8, and Iba1, tissue sections underwent antigen retrieval in a prediluted Cell Conditioning Solution (CC1; Ventana Medical Systems) for 32 min. For anti-CD8, a biotinylated secondary rabbit anti-goat antibody (1:400; BA-5000; Vector Laboratories) was applied for 10 min, whereas for anti-IRF4 the OmniMap anti-rabbit HRP kit (Ventana Medical Systems) was used for detection. Discovery Fast Red was the chromogen for CD8 and ChromoMap DAB for IRF4, B220, and CD4 (both from Ventana Medical Systems).

### Macrophage differentiation and *C. difficile* infection

Macrophages were differentiated by culturing bone marrow progenitor cells in IMDM (Lonza) containing 10% (vol/vol) heat-inactivated FBS, 30% (vol/vol) L929 cell-conditioned medium, 1% (vol/vol) nonessential amino acids (Lonza), 100 U/ml penicillin, and 100 mg/ml streptomycin at 37°C in a humidified atmosphere containing 5% CO<sub>2</sub> for 6 d. BMDMs were then seeded into  $\mu$ -Slide 8-well (Ibidi) or in multiple well plates as needed in IMDM containing 10% FBS, 1% nonessential amino acids, and antibiotics. *C. difficile* strain VPI10463 (toxigenic; TcdA<sup>+</sup>TcdB<sup>+</sup>) was purchased from ATCC. Glycerol stocks were cultured overnight at 37°C in anaerobic conditions in BHIS (brain-heart infusion supplemented with yeast extract)-enriched medium (37 g/liter brain-heart infusion, Gibco; 5 g/liter yeast extract, Gibco; 0.03% L-cysteine, Sigma; 0.1% sodium taurocholate, Sigma). Infections were performed at 10 multiplicity of infection (MOI).

### Cell death kinetic measurements (IncuCyte)

Sytox green permeability was used to quantify pyroptosis over time using CellEvent Caspase3/7 green substrate (Invitrogen) according to the manufacturer's instructions. Data were acquired and analyzed using the IncuCyte Zoom system (Essenbio) over a time span of 25 h. Each condition was run in (technical) duplicates.

### Western blotting

Unless otherwise stated, cell lysates and culture supernatants were combined for Western blotting. Protein samples were denatured in Laemmli buffer, boiled at 95°C for 10 min, separated by SDS-PAGE, and transferred to polyvinylidene difluoride membranes. PBS supplemented with 0.05% Tween-20 (vol/vol) and 3% nonfat dry milk (wt/vol) was used for blocking and washing of membranes. Immunoblots were incubated overnight with primary antibodies against caspase-1 (AG-20B-0042-C100; 1:1,000; Adipogen), GSDMD (1:1,000; Genentech; Aglietti et al., 2016), or IL-1 $\beta$  (GTX74034; 1:3,000; Genetex), followed by HRP-conjugated secondary antibodies raised against mouse, goat, or rabbit (1:5,000). The  $\beta$ -actin-HRP antibody was used at 1:5,000 in PBS 0.1% Tween-20 and 5% nonfat dry milk. All proteins were detected by enhanced chemiluminescence.

## Cytokine analysis

Cytokine levels were determined in serum and cell culture supernatants by magnetic bead-based multiplex assay using Luminesx technology (Bio-Rad) and ELISA kits that were obtained from eBiosciences and Millipore, respectively. GraphPad Prism 6.0 software was used for data analysis. Data are represented with standard deviation (SD).

## Statistical analysis

Statistical analysis was performed using GraphPad Prism 6.05 software. Student's *t* test or one-way ANOVA was used with Fischer's least significance difference or Dunn's posttest, as indicated. Two-way ANOVA was used to analyze the kinetics of body weight gain and spleen composition. In most analyses, *Mefv*<sup>V726A/+</sup> mice were used as a control to analyze the degree of disease or protection. *P*-value < 0.05 was considered significant.

## Online supplemental material

Fig. S1 shows that GSDMD is critical for IL-1 $\beta$ -dependent systemic inflammatory cytokine production in *Mefv*<sup>V726A/V726A</sup> mice. Fig. S2 shows that caspase-1 and GSDMD are cleaved in granulocytes of *Mefv*<sup>V726A/V726A</sup> mice. Fig. S3 shows the histology scores and inflammatory tissue damage in *Mefv*<sup>V726A/V726A</sup> mice from the representative sections of H&E-stained tissues provided in main Fig. 4 C.

## Acknowledgments

We thank Dr. Daniel L. Kastner for *Mefv*<sup>V726A/+</sup> mice, and Dr. Vishva M. Dixit and Dr. Nobuhiko Kayagaki for *GSDMD*<sup>-/-</sup> mice.

Part of this work was supported by European Research Council grant 683144 (PyroPop) and the Baillet Latour Medical research grant to M. Lamkanfi.

The authors declare no competing financial interests.

Author contributions: A. Kanneganti and M. Lamkanfi conceptualized the project; A. Kanneganti, R.K.S. Malireddi, P.H.V. Saavedra, L. Vande Walle, H. Van Gorp, H. Kambara, H. Tillman, H.R. Luo, and P. Vogel performed experiments; A. Kanneganti and M. Lamkanfi analyzed data and wrote the manuscript; H. Chi and R. Xavier edited the manuscript and provided mentoring, resources, and overall supervision; M. Lamkanfi coordinated the research.

Submitted: 13 November 2017

Revised: 20 March 2018

Accepted: 30 April 2018

## References

Aglietti, R.A., A. Estevez, A. Gupta, M.G. Ramirez, P.S. Liu, N. Kayagaki, C. Ciferri, V.M. Dixit, and E.C. Dueber. 2016. Gsdmd p30 elicited by caspase-11 during pyroptosis forms pores in membranes. *Proc. Natl. Acad. Sci. USA*. 113:7858–7863. <https://doi.org/10.1073/pnas.1607769113>

Andrej, C., C. Dazzi, L. Lotti, M.R. Torrisi, G. Chimini, and A. Rubartelli. 1999. The secretory route of the leaderless protein interleukin 1 $\beta$  involves exocytosis of endolysosome-related vesicles. *Mol. Biol. Cell*. 10:1463–1475. <https://doi.org/10.1091/mbc.10.5.1463>

Brydges, S.D., J.L. Mueller, M.D. McGeough, C.A. Pena, A. Misaghi, C. Gandhi, C.D. Putnam, D.L. Boyle, G.S. Firestein, A.A. Horner, et al. 2009. Inflammation-mediated disease animal models reveal roles for innate but not adaptive immunity. *Immunity*. 30:875–887. <https://doi.org/10.1016/j.immuni.2009.05.005>

Chae, J.J., Y.H. Cho, G.S. Lee, J. Cheng, P.P. Liu, L. Feigenbaum, S.I. Katz, and D.L. Kastner. 2011. Gain-of-function Pyrin mutations induce NLRP3 protein-independent interleukin-1 $\beta$  activation and severe autoinflammation in mice. *Immunity*. 34:755–768. <https://doi.org/10.1016/j.immuni.2011.02.020>

Ding, J., K. Wang, W. Liu, Y. She, Q. Sun, J. Shi, H. Sun, D.C. Wang, and F. Shao. 2016. Pore-forming activity and structural autoinhibition of the gasdermin family. *Nature*. 535:111–116. <https://doi.org/10.1038/nature18590>

Gaidt, M.M., T.S. Ebert, D. Chauhan, T. Schmidt, J.L. Schmid-Burgk, F. Rapino, A.A. Robertson, M.A. Cooper, T. Graf, and V. Hornung. 2016. Human Monocytes Engage an Alternative Inflammation Pathway. *Immunity*. 44:833–846. <https://doi.org/10.1016/j.immuni.2016.01.012>

Gao, W., J. Yang, W. Liu, Y. Wang, and F. Shao. 2016. Site-specific phosphorylation and microtubule dynamics control Pyrin inflammasome activation. *Proc. Natl. Acad. Sci. USA*. 113:E4857–E4866. <https://doi.org/10.1073/pnas.1601700113>

Garlanda, C., C.A. Dinarello, and A. Mantovani. 2013. The interleukin-1 family: back to the future. *Immunity*. 39:1003–1018. <https://doi.org/10.1016/j.immuni.2013.11.010>

Gurung, P., and T.D. Kanneganti. 2016. Autoinflammatory Skin Disorders: The Inflammasome in Focus. *Trends Mol. Med.* 22:545–564. <https://doi.org/10.1016/j.molmed.2016.05.003>

He, W.T., H. Wan, L. Hu, P. Chen, X. Wang, Z. Huang, Z.H. Yang, C.Q. Zhong, and J. Han. 2015. Gasdermin D is an executor of pyroptosis and required for interleukin-1 $\beta$  secretion. *Cell Res.* 25:1285–1298. <https://doi.org/10.1038/cr.2015.139>

Hoffman, H.M., and L. Broderick. 2016. The role of the inflammasome in patients with autoinflammatory diseases. *J. Allergy Clin. Immunol.* 138:3–14. <https://doi.org/10.1016/j.jaci.2016.05.001>

Jorgensen, I., and E.A. Miao. 2015. Pyroptotic cell death defends against intracellular pathogens. *Immunol. Rev.* 265:130–142. <https://doi.org/10.1111/immr.12287>

Jorgensen, I., Y. Zhang, B.A. Krantz, and E.A. Miao. 2016. Pyroptosis triggers pore-induced intracellular traps (PITs) that capture bacteria and lead to their clearance by efferocytosis. *J. Exp. Med.* 213:2113–2128. <https://doi.org/10.1084/jem.20151613>

Kayagaki, N., I.B. Stowe, B.L. Lee, K. O'Rourke, K. Anderson, S. Warming, T. Cuellar, B. Haley, M. Roose-Girma, Q.T. Phung, et al. 2015. Caspase-11 cleaves gasdermin D for non-canonical inflammasome signalling. *Nature*. 526:666–671. <https://doi.org/10.1038/nature15541>

Lamkanfi, M., and V.M. Dixit. 2014. Mechanisms and functions of inflammasomes. *Cell*. 157:1013–1022. <https://doi.org/10.1016/j.cell.2014.04.007>

Lamkanfi, M., A. Sarkar, L. Vande Walle, A.C. Vitari, A.O. Amer, M.D. Wewers, K.J. Tracey, T.D. Kanneganti, and V.M. Dixit. 2010. Inflammasome-dependent release of the alarmin HMGB1 in endotoxemia. *J. Immunol.* 185:4385–4392. <https://doi.org/10.1049/jimmunol.1000803>

MacKenzie, A., H.L. Wilson, E. Kiss-Toth, S.K. Dower, R.A. North, and A. Surprenant. 2001. Rapid secretion of interleukin-1 $\beta$  by microvesicle shedding. *Immunity*. 15:825–835. [https://doi.org/10.1016/S1074-7613\(01\)00229-1](https://doi.org/10.1016/S1074-7613(01)00229-1)

Man, S.M., and T.D. Kanneganti. 2016. Converging roles of caspases in inflammasome activation, cell death and innate immunity. *Nat. Rev. Immunol.* 16:7–21. <https://doi.org/10.1038/nri.2015.7>

Masters, S.L., V. Lagou, I. Jéru, P.J. Baker, L. Van Eyck, D.A. Parry, D. Lawless, D. De Nardo, J.E. Garcia-Perez, L.F. Dagley, et al. 2016. Familial autoinflammation with neutrophilic dermatosis reveals a regulatory mechanism of pyrin activation. *Sci. Transl. Med.* 8:332ra45. <https://doi.org/10.1126/scitranslmed.aaf1471>

Ozdogan, H., and S. Ugurlu. 2017. Canakinumab for the treatment of familial Mediterranean fever. *Expert Rev. Clin. Immunol.* 13:393–404. <https://doi.org/10.1080/17446666X.2017.1313116>

Ozen, S., and Y. Bilginer. 2014. A clinical guide to autoinflammatory diseases: familial Mediterranean fever and next-of-kin. *Nat. Rev. Rheumatol.* 10:135–147. <https://doi.org/10.1038/nrrheum.2013.174>

Park, Y.H., G. Wood, D.L. Kastner, and J.J. Chae. 2016. Pyrin inflammasome activation and RhoA signaling in the autoinflammatory diseases FMF and HIDS. *Nat. Immunol.* 17:914–921. <https://doi.org/10.1038/ni.3457>

Qu, Y., L. Franchi, G. Nunez, and G.R. Dubyak. 2007. Nonclassical IL-1 $\beta$  secretion stimulated by P2X7 receptors is dependent on inflammasome

- activation and correlated with exosome release in murine macrophages. *J. Immunol.* 179:1913–1925. <https://doi.org/10.4049/jimmunol.179.3.1913>
- Ridker, P.M., B.M. Everett, T. Thuren, J.G. MacFadyen, W.H. Chang, C. Ballantyne, F. Fonseca, J. Nicolau, W. Koenig, S.D. Anker, et al. CANTOS Trial Group. 2017a. Antiinflammatory Therapy with Canakinumab for Atherosclerotic Disease. *N. Engl. J. Med.* 377:1119–1131. <https://doi.org/10.1056/NEJMoa1707914>
- Ridker, P.M., J.G. MacFadyen, T. Thuren, B.M. Everett, P. Libby, and R.J. Glynn. CANTOS Trial Group. 2017b. Effect of interleukin-1 $\beta$  inhibition with canakinumab on incident lung cancer in patients with atherosclerosis: exploratory results from a randomised, double-blind, placebo-controlled trial. *Lancet.* 390:1833–1842. [https://doi.org/10.1016/S0140-6736\(17\)32247-X](https://doi.org/10.1016/S0140-6736(17)32247-X)
- Sharma, D., B.R. Sharma, P. Vogel, and T.D. Kanneganti. 2017. IL-1 $\beta$  and Caspase-1 Drive Autoinflammatory Disease Independently of IL-1 $\alpha$  or Caspase-8 in a Mouse Model of Familial Mediterranean Fever. *Am. J. Pathol.* 187:236–244. <https://doi.org/10.1016/j.ajpath.2016.10.015>
- Shi, J., Y. Zhao, K. Wang, X. Shi, Y. Wang, H. Huang, Y. Zhuang, T. Cai, F. Wang, and F. Shao. 2015. Cleavage of GSDMD by inflammatory caspases determines pyroptotic cell death. *Nature.* 526:660–665. <https://doi.org/10.1038/nature15514>
- Vande Walle, L., and M. Lamkanfi. 2016. Pyroptosis. *Curr. Biol.* 26:R568–R572. <https://doi.org/10.1016/j.cub.2016.02.019>
- Vande Walle, L., N. Van Opdenbosch, P. Jacques, A. Fossoul, E. Verheugen, P. Vogel, R. Beyaert, D. Elewaut, T.D. Kanneganti, G. van Loo, and M. Lamkanfi. 2014. Negative regulation of the NLRP3 inflammasome by A20 protects against arthritis. *Nature.* 512:69–73. <https://doi.org/10.1038/nature13322>
- Van Gorp, H., P.H. Saavedra, N.M. de Vasconcelos, N. Van Opdenbosch, L. Vande Walle, M. Matusiak, G. Prencipe, A. Insalaco, F. Van Hauwermeiren, D. Demon, et al. 2016. Familial Mediterranean fever mutations lift the obligatory requirement for microtubules in Pyrin inflammasome activation. *Proc. Natl. Acad. Sci. USA.* 113:14384–14389. <https://doi.org/10.1073/pnas.1613156113>
- Van Gorp, H., N. Van Opdenbosch, and M. Lamkanfi. 2017. Inflammasome-dependent cytokines at the crossroads of health and autoinflammatory disease. *Cold Spring Harb. Perspect. Biol.*:a028563. <https://doi.org/10.1101/cshperspect.a028563>
- Xu, H., J. Yang, W. Gao, L. Li, P. Li, L. Zhang, Y.N. Gong, X. Peng, J.J. Xi, S. Chen, et al. 2014. Innate immune sensing of bacterial modifications of Rho GTPases by the Pyrin inflammasome. *Nature.* 513:237–241. <https://doi.org/10.1038/nature13449>